International Journal of Rock Mechanics & Mining Sciences 170 (2023) 105484

Contents lists available at ScienceDirect

International Journal of Rock Mechanics and Mining Sciences

journal homepage: www.elsevier.com/locate/ijrmms

Numerical studies of floor heave mechanism and the effectiveness of grouting reinforcement of roadway in soft rock containing the mine water

Ivan Sakhno *, Svitlana Sakhno

Donetsk National Technical University, 29, Sofia Kovalevska Street, Lutsk, Volyn region, 43012, Ukraine

ARTICLE INFO

Keywords:
Mine roadways
Floor heave
Moisture content
Soft rock
Numerical modelling
Stress
Strain
Grouting reinforcement

ABSTRACT

A floor heave is a serious failure phenomenon in mining roadways, especially in soft rock containing the mine water. Considering the influences of moisture content on rock properties, a case study of the floor heave mechanism and grouting control technology was performed in this paper. The results of laboratory tests showed that with the increase of moisture content, the compressive strength and friction angle of mudstone linearly decreased, while the deformation modulus and cohesion tended to a negative exponential decrease approximately. A numerical simulation was used to study the stress and strain distributions of the surrounding rock. It was found that significant floor heave was caused plastic deformation of mudstone under high moisture content. In the case of large floor heave a "core" of vertical expansion is formed in the floor strata. This area of the surrounding rocks is mainly involved in the development of floor heave. Grouting reinforcement was proposed to control the floor heave. Five grouting schemes with different depth of reinforcement were studied. The numerical simulation demonstrated that after grouting reinforcement, plastic strain in the floor strata was reduced effectively. The minimum required grouting depth is determined by the allowable floor heave and moisture content. Ideally, the floor heaves could be reduced when the grouting depth is greater than the area where the "core" of vertical expansion appears.

1. Introduction

Coal resources play an important role in the energy structure, more than a quarter of the world's primary energy is provided using coal.[1] The coking coals required by metallurgy are still in high demand. With the exhaustion of shallow coal resources, the geological conditions of mining are gradually deteriorating. Under the influence of high geostress the failure zone around the roadways increases. This causes large deformations of the surrounding rock, the destruction of support systems, and multiple repairs of roadways. In the case of the rock mass composed of soft mudstone, sandy mudstone, argillaceous sandstone, the stability of the roadways is further reduced. Such rocks are composed of clay minerals with water-absorbent properties, and have numerous cracks, making them weak.

Support of roadways, including steel arch, bolting, and hydraulic supports, are commonly successfully used to control the deformation of roof and side wall of roadways. Control of floor deformation of roadways is less successful, therefore a floor heave to be a serious failure phenomenon in mine roadways, especially in conditions of increased water inflows.[2–4] At the same time, during designing roadway excavations in rock mass exposed to floor uplift, three criteria should be taken into account: geometrical machinery and equipment, ventilation and geomechanical loads.[5] Therefore, it is of great significance to study the floor heave control of roadways.

Many studies have been conducted on the different mechanism of floor heave. These studies can be divided into four groups: extrusion flow, flexure fold, shear dislocation, and water-induced swelling.[2,6–8] The development of floor heave is greatly influenced by horizontal stresses. The floor heave mechanism at different stages of exploitation roadway may be different.

There are three dominant technologies of floor heave controlling: using the steel closed support (inverted arch, circular etc.), cutting stress relief slot in the floor or wall of roadway, reinforcing of surrounding rock (bolts, anchor cables, grouting etc.). The combinations of the listed methods are often used.

Zhao et al.[9] researched and proposed a mechanical model for controlling floor heave with the U-shaped steel closed support. Wang et al.[10] managed to control floor heave by using the high resistance yieldable

* Corresponding author.
E-mail address: ivan.sakhno@donntu.edu.ua (I. Sakhno).

https://doi.org/10.1016/j.ijrmms.2023.105484
Received 7 October 2022; Received in revised form 6 April 2023; Accepted 20 June 2023
Available online 4 July 2023

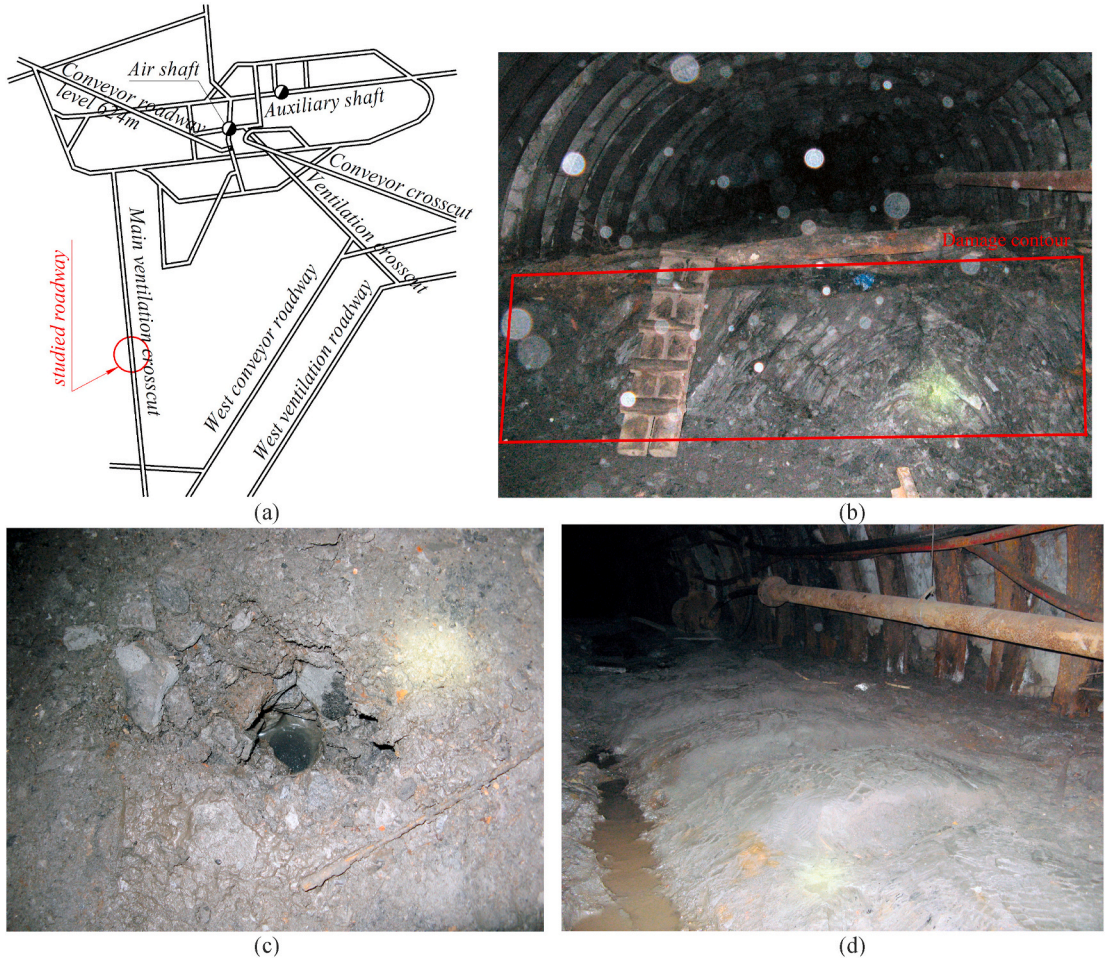

Fig. 1. The studied area and the conditions of the roadway (a) the locations of studied roadway; (b) the dramatic floor heave in roadway; (c) the observation boreholes with water; (d) the floor surface of roadway.

multiple support for roadways excavated in extremely soft rocks. A case study is also presented the application of the principles for controlling the roadway stability control of roadways excavated in soft rocks using a multiple support system with joints. Wang et al.[11] proposed new steel circular closed support with I-section of sinusoidal corrugated webs to mitigate large deformation of roadways in soft rock.

Chen et al.[12] put forward the innovative "relief-retaining" control scheme of floor heave. The "relief-retaining" control scheme of floor heave is proposed, which is the comprehensive measure of cutting groove in floor + drilling for pressure relief at roadway side + setting retaining piles at the junction of roadway side and floor. The types of slots can be a groove or a borehole. A pressure relief groove is cut in the floor in longitudinal axis of the roadway or in two corners on the floor.[13] The hole is usually located along the longitudinal axis, while its depth is much bigger than that one of the groove and can be several meters deep.[13] This method is technically difficult for implementation, moreover, it is expensive. Therefore, it is not widely used these days.

One of the most perspective technologies is the one of reinforcing the floor of a roadway. He et al.[14] proposed the bolt, and anchor coupling support technology to control the large deformation and floor heave of deep coal roadway. Yang et al.[15] studied the floor heave control method of high-stress soft rock roadway, and proposed new coupling support technology of a bolt-mesh-anchor-base angle bolt-flexible layer truss for controlling roadway floor heave. Wang et al.[16] using numerical simulations and theoretical analysis determined that an effective method for controlling floor heave is "self-drilling anchor bolt" + "high-strength reinforcement anchor bolt" + "W type steel belt" + "steel mesh" + anchor cable with birdcage. Chang et al.[17] designed reasonable support parameters of hydraulic expansion bolts, which can reduce the plastic zone in the floor.

Cement grouting is an effective floor reinforcement technique that can control dramatic floor heaves. So far, the grouting reinforcement technique has been widely used in roadway support. Shimada et al.[18] studied the reinforcement effect of cement grouting materials with different water–cement ratios on the floor. Zhang et al.[19] managed to control floor heave in retained goaf-side gateroad by using grouting reinforcement. Gong et al.[20] on the basis of field test and monitoring results showed that the comprehensive control scheme of adjusting backfilling pressure, deep grouting reinforcement can effectively control the floor heave of the gob-backfilled gob-side entry retaining.

The prospect of floor heave control by grouting reinforcement is a very attractive, but the high efficiency of this technology is not always achieved. In soft rock considering the mine water, some additional measures and update of reinforcing methods are required. For example, in the works[18,21] it is shown that the quality of reinforcing increases with dehydration of water-saturated rocks. The studies of the effect of water on the floor heave were undertaken in the work.[22] Sun et al. and Zhong et al. put forward the technology of reinforcing surrounding rocks to realize the floor stability in inclined strata and soft rock.[23,24]

Numerical simulation on the floor heave mechanism in roadway with soft rock has been widely used in the previous studies. Chen et al.,[12] Zhang et al.,[19] Zhu et al.,[25] explored the evolution of stress at the floor of roadways by FLAC^{3D}. Tang et al.[22] simulated the floor heave processes of a swelling rock under the high humidity by RFPA. Zhang et al.[7] and

Table 1
Physical and mechanical parameters of surrounding rock.

N°	Rock Strata	Density (kg/m^3)	Compressive strength (MPa)	Tensile strength (MPa)	Young's modulus (GPa)	Poisson's ratio
1	Sandy mudstone	2400	21.4	2.1	6.6	0.29
2	Mudstone	2300	18.7	1.8	1.8	0.3

Shen[12] simulated the failure mechanism of soft rock roadway by UDEC. Sakhno et al.[26] performed numerical modelling of controlling a floor heave of roadways in wet soft rock by Ansys.

In this paper, the floor heave mechanism and grouting reinforcement technology of roadway were studied to effectively control the large plastic deformation of soft floor rock containing the mine water. The influence of the moisture content on the mechanical properties of the mudstone was studied using laboratory tests. With the change of moisture content, the floor heave and development of plastic zone in surrounding rocks were analyzed by the Ansys. This paper puts forward the 2 elements scheme to control the floor heave. The specific parameters suitable for controlling the floor heave of cross-cut are determined using numerical simulation method.

2. Engineering background

2.1. Engineering geological conditions

A project was conducted in Surgaya coal mine, Ukraine. This is a typical Ukrainian underground coal mine with a depth of 800 m in Vugledar city, Donbass region. The studied roadway is shown in Fig. 1a. It was main ventilation cross-cut for return-air from the west wing of level 624 m. The section shape of the roadway was a semi-circular arch, 5.2 m in width and 4.8 m in height. The height of the straight wall was 1.8 m and the radius of the arch was 3.05 m. The support used in roadway was U-shape steel arches (U33) with concrete insert plates. The floor of roadway was not supported. The track cross-cut was surrounded mainly by mudstone and less often by sandy mudstone. The rock mass properties are shown in Table 1. The average compressive strength of mudstone and sandy mudstone was 18.7 MPa and 21.4 MPa, respectively. The International Society for Rock Mechanics (ISRM) classifies rocks with a uniaxial compressive strength (UCS) of 5–25 MPa as "weak" (ISRM 1981).[27] Kanji 2014[28] considers that the upper limit of strength of what is called "soft" rock is about 25 MPa in the form of unconfined compressive strength. According to these classifications, surrounding rocks were weak and soft rocks.

Due to the previous long exploitation time of gateroad (more than 10 years), surrounding soft rocks was full of fractures and cracks. Therefore, large deformation of surrounding rock appeared. The gateroad was reconstructed several times. After each reconstruction, the surrounding rock of the roadway always kept a high failure degree over time. Six months after reconstruction the average roof subsidence and side walls convergence were 405 mm and 310 mm, respectively. In some areas, the accumulative deformation was as large as 1.3–1.5 times. Despite this, the deformations of the roof and side walls were not critical. In the cross-cut was a dramatic floor heave up to 1.0 m (Fig. 1b). Even attempts to use an inverted arch steel support did not help to effectively control this deformation. The floor heave was aggravated by the high water content of the rocks. The observation boreholes were filled with water, which indicated high moisture of the floor rocks (Fig. 1c). The mudstone on the

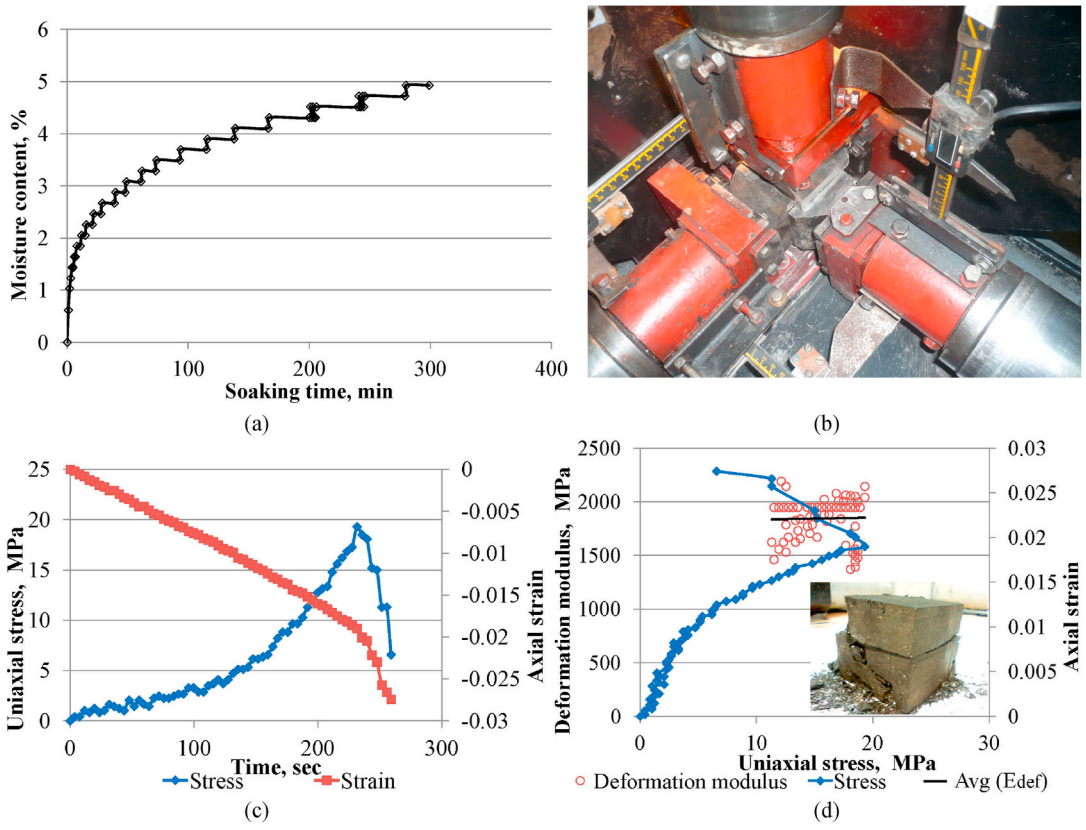

Fig. 2. Laboratory test results and equipment (a) the variation in moisture content with time in soaking; (b) the universal testing machine; (c) time-stress and time-strain curves for a "dry" specimen; (d) time-strain curve and deformation modulus fluctuations for a "dry" specimen.

Table 2
Technical specifications of universal testing machine.

Specification	UNTS
Load measurement accuracy	1%
Displacement measurement accuracy	0.01 mm
Test chamber dimensions max/min	60 × 60 × 60 mm/50 × 50 × 50 mm
Max pressure	100 MPa
Pistons stroke	100 mm
Data reading frequency	0.5–5 1/c

floor surface were swollen and softened, similar in texture to clay (Fig. 1d).

Due to moisture, the strength of the surrounding rocks gradually decreased over time. The deformation properties also changed. This contributed to the development of large deformations in the gateroad. The ventilation of the mine depends on the deformations degree of the cross-cut and especially on the rate of floor heave. Therefore, it is imminent to research the control technology of the cross-cut floor heave.

2.2. The influence of moisture on rock properties

The phenomenon of decrease of mechanical rock properties when they are moistened is well known.[29] It explains the critical floor heave in areas of high humidity, repeatedly recorded in-situ.[20,30,31] Several studies have found a significant decrease in (UCS) and Young's modulus with increasing humidity in sandstones,[32–34] limestones and mudstones.[35–37] The decrease in UCS depending on the content, structure and petrological characteristics of rocks usually varies within 9–65%, and the decrease in Young's modulus is 15–77%. Rabat et al.[38] obtained significant cohesion reductions (of 9% in sandstones and of 35–53% in limestones) and also significant friction angles decreases (of 14% and of 5–22%, for sandstones and limestones, respectively). Studies of mudstones[39] have shown a decrease in the angle of friction up to 26%, a decrease in cohesion up to 67%. Brazilian tensile strength (BTS) and shear strength parameters are less studied. Ojo and Brook[20] and Karakul and Ulusay,[21] reported reductions BTS up to 50 and 63% in sandstones, respectively. Chen et al.[39] have found a shear strength reduction of up to 81% for mudstones.

The study was carried out for mudstone, as it is softer than sandy mudstone and more common along the roadway. The influence of the amount of water contained inside the rocks on the properties of the mudstone was studied using laboratory tests on cube-shaped specimens with a rib size of 55 mm. First of all specimens had been placed in a drying oven for 24 h. After that, their mass was measured. This mass corresponded to "dry" specimens. Subsequently, specimens for various times were placed in a box with water. After a period of soaking time, specimens were removed and weighted. This made possible to calculate their moisture contents. The results of the soaking testing are summarized in Fig. 2a.

After wiping free water from the surface of the specimens, they were tested on a universal testing machine (Fig. 2b). The technical characteristics of the universal testing machine[40] are shown in Table 2. Test results for a "dry" specimen are shown in (Fig. 2c) as an example. Then, the average strain modulus was calculated in the middle section of the stress-strain curve. The deformation modulus fluctuations for a "dry" specimen in the load range of 10–18.7 MPa are shown in Fig. 2d. The average value of the deformation modulus is 1800 MPa. Finally, the values of the angle of friction and cohesion were calculated.

The compressive strengths (σ_c) and deformation modulus (E_{def}) evolution laws with the moisture content (w) were shown in Fig. 3a. It is seen that the compressive strength decreases with the increase of moisture content. To describe the relationship between moisture content and compressive strengths was proposed linear function $\sigma_c = -2.0477w + 20.23$ ($R^2 = 0.88$). It is seen that the deformation modulus decreases nonlinearly with the increase of moisture content. The relationship between deformation modulus and moisture content was described negative exponential function $E_{def} = 2.2416e^{-0,335w}$ ($R^2 = 0.96$).

Fig. 3b shows the influences of moisture content on cohesion (c), and friction angle (φ) of mudstone. It is seen that friction angle decreases linearly, while cohesion decreases nonlinearly with the increase of moisture content. The relationships between moisture content, mudstone cohesion, and friction angle are shown in the following equation.

$$c = 4.2689e^{-0,213w} \ (R^2 = 0.98),$$
$$\varphi = -1.3417w + 28.112 \ (R^2 = 0.98).$$

Several authors have proposed negative exponential, power or linear functions to describe the relationship between moisture content (w) and UCS.[35,37,41–47] Same correlation function types are proposed to describe the variations of E and BTS with moisture content. Thus, this experience coincides with the presented studies, which confirms their validity. The correlations proposed above were used in the numerical analysis.

The conducted studies allow to accurately describe the relationship of physical and mechanical properties from humidity for the tested mudstones in a single loading mode. However, the changes in the geomechanical properties of rocks after soaking are function of their mineralogical composition, as shown by Malkowski et al.[48] Therefore, conducting research in other conditions, it is necessary to conduct additional tests of rocks. In addition, the rock mechanical parameters depend on strain-stress state. Therefore, when conducting research in other conditions, it is necessary to conduct additional tests of rocks. In general, the reduction of mechanical parameters of rock after wetting is known and confirmed by other researchers.[49]

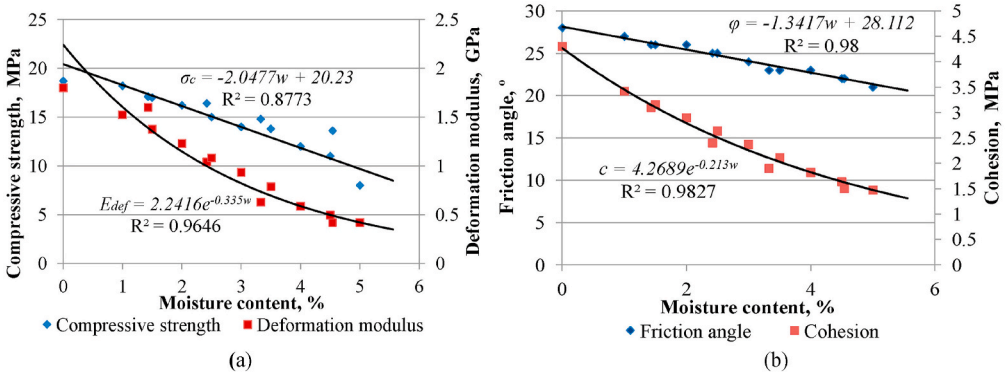

Fig. 3. Influence of moisture content (w) on the compressive strength (σ_c) and deformation modulus (E_{def}) (a), friction angle (φ) and cohesion (c) (b) of mudstone.

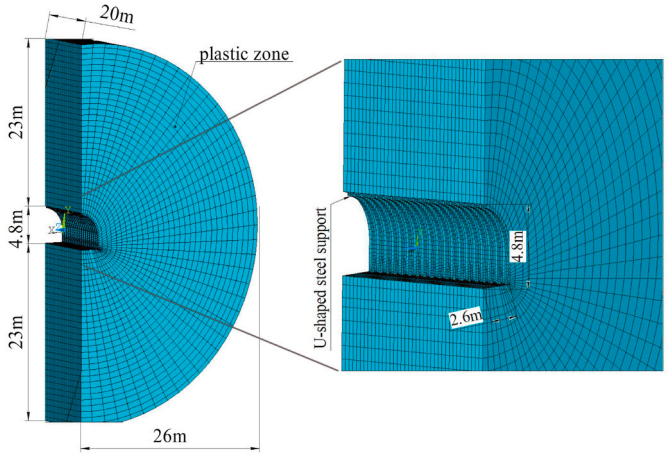

Fig. 4. Numerical calculation model.

3. Study of the floor heave in soft rock containing the mine water

3.1. Numerical model

Deformation and instability of deep roadways today are well studied. These processes are associated with the formation of a non-elastic zone around the roadway, which was described in detail in the work.[50–52] True "three-zones" (fracture zone, plastic zone and elastic zone) failure model of the surrounding rock formed by a stress redistribution which was caused by roadway excavation, often simplified to the "two-zones" (plastic failure zone and elastic zone) failure model.[50,54] The previous research[53,55,56] shows a close relation between the range and shape of the plastic zone and the stability of the roadway. Extending of the plastic zone under the external pressure (or as a result of excavating of rock during reconstruction of roadway), leads to increase of unrestrained deformations.[17,57–59] Extending of the plastic zone is accompanied by the destruction of rocks on its contour.These considerations formed the basis of the numerical model.

The ANSYS code was used. The ANSYS software can effectively simulate the large plastic deformation problem of the underground engineering including the prestress effect. To simulate the behavior of soils and rocks in ANSYS, the Drucker-Prager model is used. The same model is used in other softwares, such as FLAC3D, ABAQUS. Drucker-Prager model commendably depicts the strength characteristics of rock and soil. The model enables simulating plastic deformation of rock and its other pressure-dependent material, which corresponds to the properties of rocks in a fracture zone. The results of studies[40,60,61] validated applicability of Drucker-Prager model to simulate the behavior of the heterogeneous rock.

Numerical model was established according to the actual cross-cut design based on the actual geological engineering conditions. The model is axisymmetric, so a half of it cross-section was modeled. To simplify the model and reduce the boundary influence, a boundary (length = 23 m) was set around the roadway. The numerical model was 20 m long, 26 m wide, and 50.8 m high (Fig. 4). A 5.2 x 4.8 m arch shape roadway was adopted, and the beam unit was used to simulate the U-shaped steel support. Yielding nodes of steel arch support were not modeled. The contact surface with friction coefficient 0.9 was created between the support and the rock mass. In this case, it is taken into account that the steel arches have a high degree of corrosion, and the roadway walls are not smooth. Horizontal displacements were fixed at the front, back and right boundaries of the model. Uniform pressure of 20 MPa equivalents to the dynamic UCS of mudstone was applied on the semicircular contour of the model, which simulated the expansion of the plastic zone.

Table 3 presents the mechanical parameters of mudstone under different moisture contents that were taken from the results of laboratory tests. In numerical simulation, whole surrounding rock contains water. Geometric and mechanical parameters of U-shaped steel support are shown in Table 4.

3.2. Simulation results

In the case of dry rock deformations of the roof, sidewall, and floor are small. Vertical and max principal strains of surrounding rock are in the limits of elasticity, except for the bottom corner of the roadway, where floor rock contacts with the leg of frame (Fig. 5 a, b, c). Original arch steel support is in acceptable load mode mainly with sliding and sticking surface contact with the rock mass (Fig. 5 d).

According to the results of testing soft rocks samples in a volumetric field[62,63] and under uniaxial compression,[64,65] it was found that for mudstone, siltstone, argillite, shale and sandstone with a strength of 25–40 MPa, the failure limit for strain is about 0.02–0.03. This is generally corresponding with the autors results of laboratory tests on mudstones (Fig. 2).

The analysis Fig. 5 shows that failure strain in the model is a negative one; they are caused by compression of rocks in the bottom corner of the roadway (Fig. 5 a, c). The plastic strain in other areas of model do not reach the failure limit, being in the range of "-0.02" - "+0.02".

Fig. 6 shows the stress distribution of the surrounding rock.

It is seen that zone of reduced stresses σ_1 (Fig. 6 a) is formed in the floor of the roadway at a depth that exceeds half of the roadway width (W), and in the side at the level of the straight wall of the roadway. In the zone, the stress σ_1 is 2–3 times less than outside the area of the roadway influence. The floor heave of the roadway is 0.06 m. The analysis of the distribution patterns of the minimum principal stresses σ_3 (Fig. 6 b) shows that a compression area of more than 30 MPa is formed around the U-shaped steel support, repeating the arch shape of sidewall and roof of roadway at a distance of up to 0.1W, which can be explained by the resistance of steel support.

Figs. 7 and 8 and **9** show the distributions of maximum principle

Table 3
Mudstone parameters for numerical simulation.

N°	Moisture content (%)	Compressive strength (MPa)	Tensile strength (MPa)	Shear modulus (GPa)	Deformation modulus (GPa)	Poisson's ratio	Cohesion value, (MPa)	Angle of internal friction (deg)	Dilatancy angle (deg)
1	0	18.7	1.8	0.72	1.8	0.3	4.3	28	28
2	1	18.2	1.45	0.65	1.52	0.3	3.42	27	27
3	1.5	17	1.28	0.51	1.38	0.3	3.16	26	26
4	2	16.2	1.12	0.43	1.23	0.3	2.89	26	26
5	2.5	15	0.96	0.36	1.08	0.3	2.63	25	25
6	3	14	0.79	0.31	0.93	0.3	2.37	24	24
8	3.5	13.8	0.63	0.26	0.79	0.3	2.11	23	23
9	4	12	0.47	0.22	0.59	0.3	1.82	23	23
10	4.5	11	0.31	0.18	0.50	0.3	1.64	22	22
11	5	8	0.14	0.16	0.42	0.3	1.47	21	21

Table 4
Properties of support elements used in the model.

Primary support	Type of elements	Material behaviour option	Elastic modulus (GPa)	Poisson's ratio	Yield strength (GPa)	Tangent modulus (MPa)	Contact cohesion (Pa)
U-shaped steel support	Beam	Bilinear isotropic hardening	200	0.3	52.2	342	78245

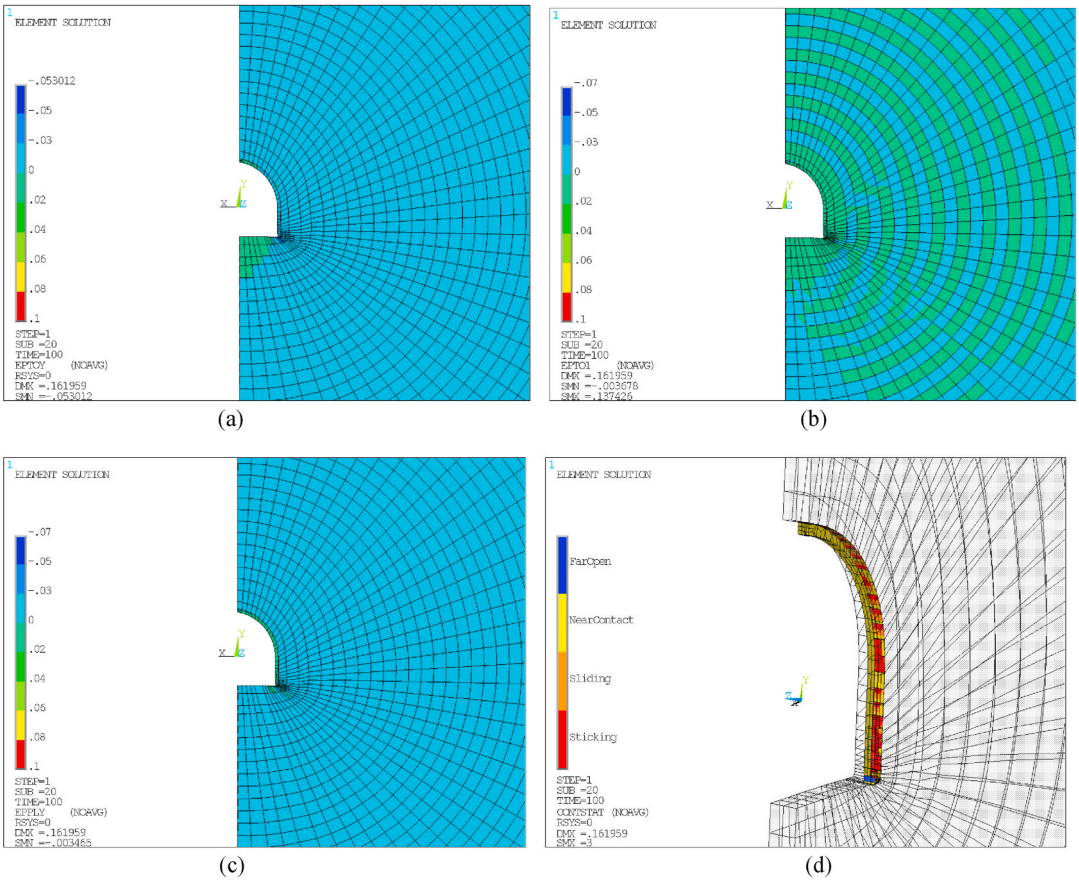

Fig. 5. The results of numerical calculation in the case of dry rock. (a) vertical elastic strain; (b) max principal strain; (c) plastic strains around the roadway; (d) contact status steel support with the rock mass.

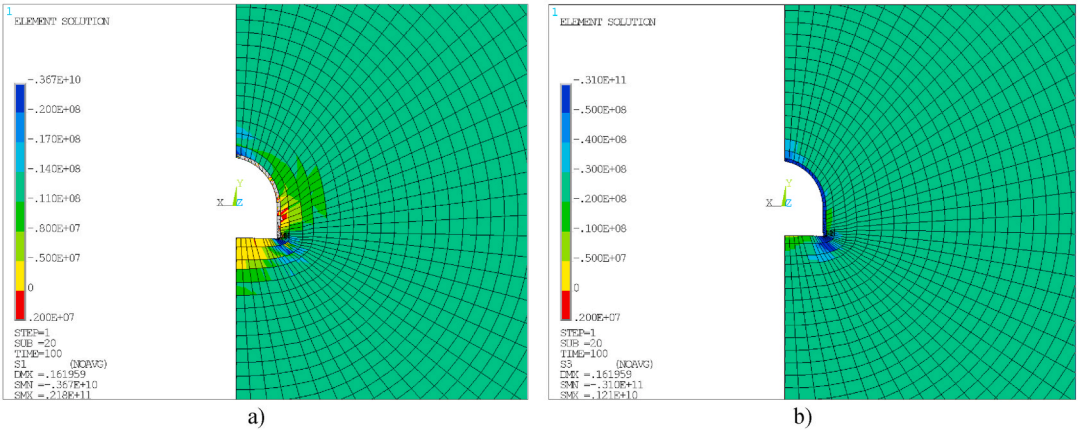

Fig. 6. Maximum (σ_1) (a) and minimum (σ_3) (b) principal stresses around the roadway in case of dry rock.

stress, maximum principle strain and minimum principle strain, respectively, for the surrounding rock with the various moisture contents.

The evolution of maximum principle stress (Fig. 7) shows that the size of the zone of reduced stress in the floor and the sidewalls of the roadway increases gradually. At the same time, as the zone of redused

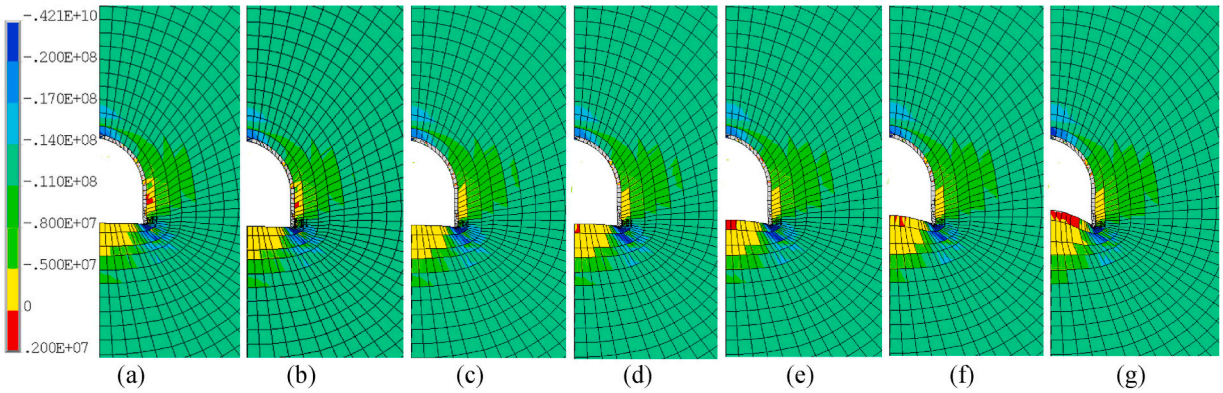

Fig. 7. Maximum principle stress distribution around the roadway under different moisture contents. (a) 1%; (b) 2%; (c) 3%; (d) 3.5%; (e) 4%; (f) 4.5%; (g) 5%.

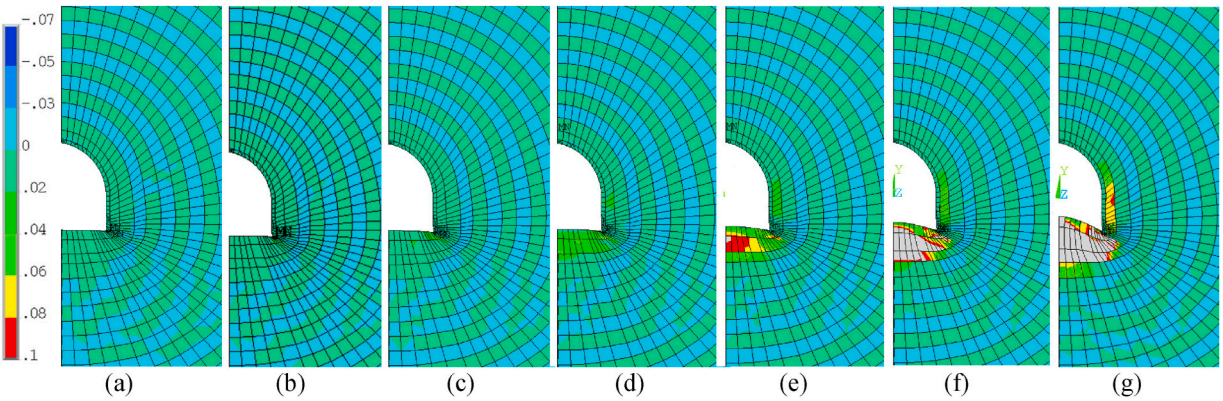

Fig. 8. Total maximum principle strain distribution around the roadway under different moisture contents. (a) 1%; (b) 2%; (c) 3%; (d) 3.5%; (e) 4%; (f) 4.5%; (g) 5%.

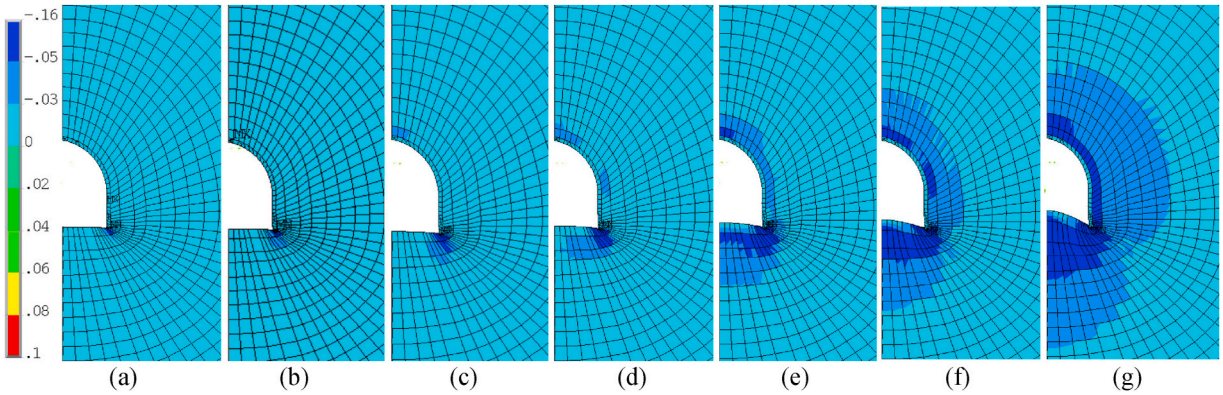

Fig. 9. Total minimum principle strain distribution around the roadway under different moisture contents. (a) 1%; (b) 2%; (c) 3%; (d) 3.5%; (e) 4%; (f) 4.5%; (g) 5%.

stress in the floor increase, in the wall sides of the roadway, the stresses become less intense. An active increase in maximum principle stress in the floor of roadway is observed at a moisture content of more than 3.5%. The size of the zone of redused stress with an increase in humidity from 1 to 5% increases to a depth from *0.5W* to *W*.

The maximum principle strain of surrounding rock of the roadway increases non-linearly with increasing moisture content, as shown in Fig. 8. With a moisture content of 3.5% or more, the maximum principle strain in floor of roadway exceeds the failure limit (+0.02). This indicates the formation of cracks in the floor rock. At the same time, at a moisture content of 4%, a "core" of vertical expansion is formed in the floor rock, at a depth of 0.5 m from the contour of the roadway. Most likely, this is caused by dilatancy and plastic flow of rocks. The vertical size of the "core" increases from 1 m to 2 m with an increase in moisture content from 4% to 5%. At the same time, positive strain in the "core" is more than 10%. The gray color shows the areas of surrounding rocks where the strain is more than 10%. At the level of the straight side wall of the roadway formes post-peak maximum principal strain at moisture content 3.5% or more. Cracks zone in the sides of the roadway reaches 1 m at moisture content of 5%; the maximum principle strain is 8–10%.

The analysis of evolution of minimum principle strain (Fig. 9) shows that the size of the failure zone, caused by compression of rock, does not grow in proportion to the increase in moisture content. Minimum principle strain at moisture content up to 3.5% is post-peak, mainly in

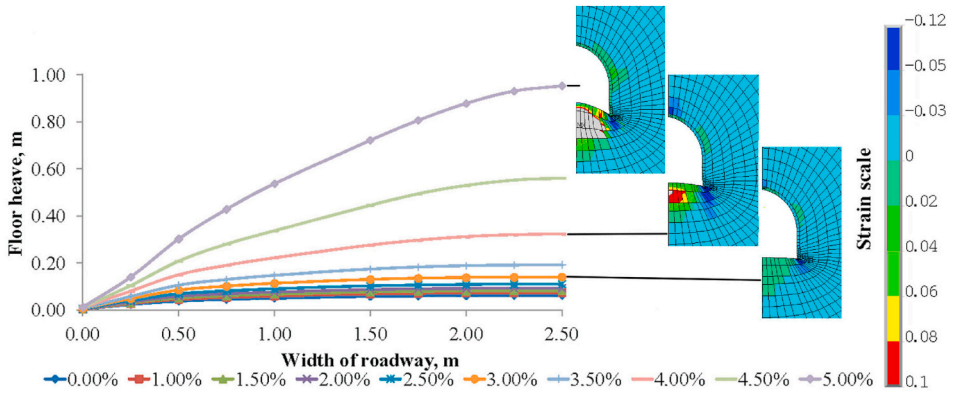

Fig. 10. Floor heave and vertical total strain distribution around the roadway under different moisture contents.

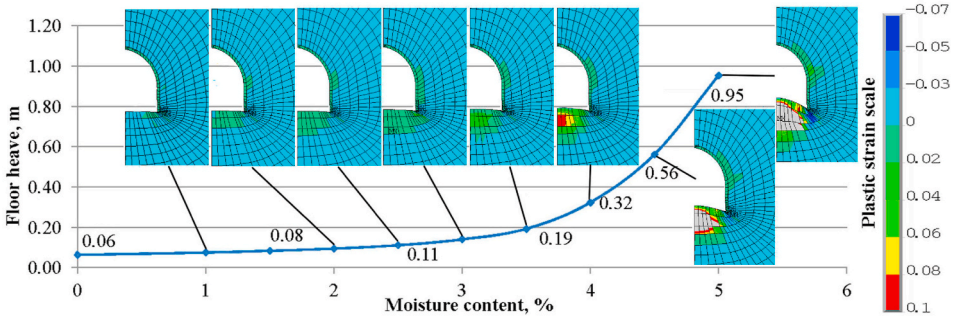

Fig. 11. Maximum floor heave and vertical plastic strain distribution around the roadway under different moisture contents.

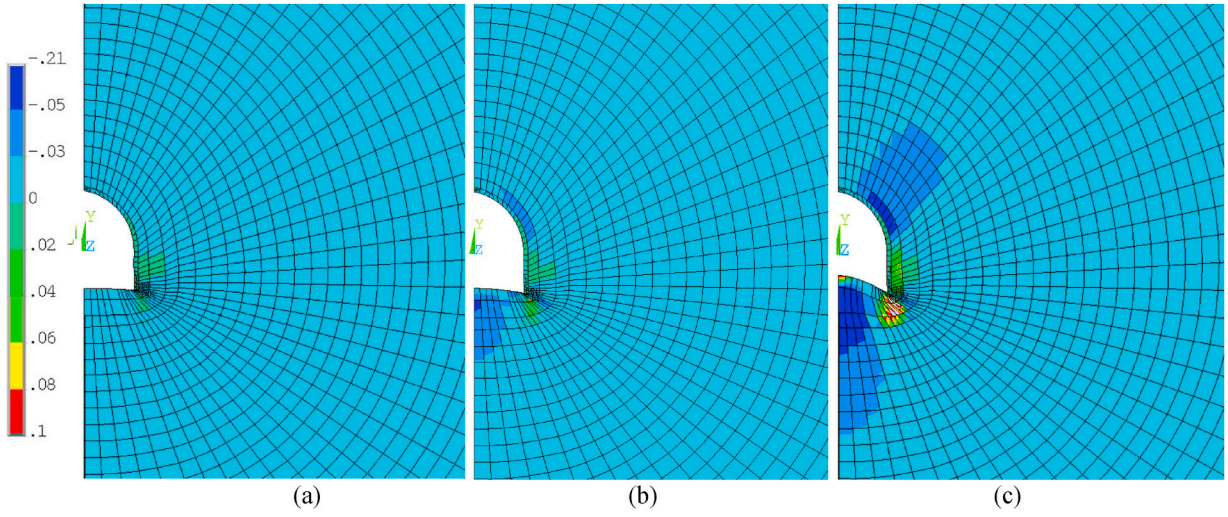

Fig. 12. Horizontal total strain distribution around the roadway under different moisture contents. (a) 3%; (b) 4%; (c) 5%.

the bottom corners of roadway. An increase in moisture content from 3.5% to 5% leads to an increase in failure zone in floor rock from 0.7 to 8.7 m. The failure zone in the sides and in the roof of the roadway reaches 5.2 m.

The influence of water content of mudstone on the amount of floor heaving can be traced according to the graphs shown in Figs. 10 and 11. The horizontal axis in Fig. 10 shows the half-width of the roadway, where the point "0″ corresponds to the bottom corner of the roadway, and the point "2.5″ corresponds to the longitudinal axis of the roadway. Fig. 10 also shows the vertical total strain distribution at 3%, 4%, 5% of moisture content. The maximum floor heave is observed along the roadway axis, which is logical.

The non-linear nature of floor heave with an increase of the moisture contents is clearly seen in the graph Fig. 11. Fig. 11 shows the evolution of floor heave on thelongitudinal axis of the roadway and vertical plastic strain distribution under different moisture contents. It is seen that non-linear increase of floor heave starts at 3%–3.5% moisture content. At the same time, the formation of a positive strain in the floor of the roadway is observed, which exceed the failure limit (+0.02). Thus, the non-linear increase in heaving is a consequence of the transition of rocks to the stage of plastic deformation.

Fig. 12 shows the horizontal total strain distribution around the roadway under moisture contents 3%, 4%, 5%. It is seen that horizontal strain in the floor of the roadway is negative. That means the rocks are

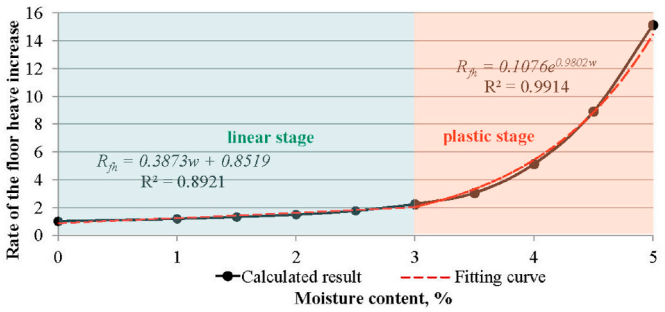

Fig. 13. The relationship between moisture content (w) and rate of the floor heave increases (R_{fh}).

compressed in the horizontal direction. Thus, the "core" that is formed in the floor of roadway is compressed horizontally and expands vertically. Horizontal strain at the same time exceeds the failure limit by 2.5–10 times.

3.3. Simulation discussions

Several conclusions can be drawn according to the above analyses.

(1) The roof and sidewalls were controlled effectively by the original steel arch support. The significant deformations in the roof and sidewalls are not observed. In this, the simulation results correspond with observations of roadway in situ.
(2) The strain analysis shows that a significant proportion of them are plastic ones (Figs. 8–11). The analysis shows that failure strains in the model are both positive and negative ones. In the wall sides and in the roof of the roadway, they are caused by the compression of rocks and have a minus sign (Fig. 9). In the floor of roadway, vertical failure strains are positive. They are mainly plastic strains. They exceed the failure limit by 3–7 times and cause the floor heave (Figs. 8 and 11). Horizontal failure strains in the floor of roadway are negative. Horizontal strains exceed the failure limit by 2.5–10 times. At the same time, at a moisture content of 4%, a "core" of vertical expansion is formed in the floor of roadway, which also contracts horizontally. This phenomenon is probably caused by dilatancy and plastic flow of rocks. At a moisture content of 5%, the depth of the vertical expansion "core" reaches 2 m. This area of the surrounding rocks is mainly involved in the development of floor heave.
(3) The critical moisture level for mudstone in the study is 3–3.5%. Plastic strain, which is the cause of uncontrolled dramatic floor heave, starts at this limit. When the moisture content of the surrounding rocks is less than 3%, the influence of moisture content on the floor heave is linear.

The ratio of floor heave value in the moisture rock (H_{fw}) to the floor heave value in the dry rock (H_{fd}) defined the rate of the floor heave increase under humidity (R_{fh}). To describe the variations of (R_{fh}) under moisture content two types of correlation function are proposed. At the first stage (0–3% moisture content) was proposed linear function $R_{fh} = 0.3873w + 0.852$ ($R^2 = 0.89$), as shown in Fig. 13. At the second stage (3–5% moisture content) the relationship between (R_{fh}) and moisture content was described by exponential function $R_{fh} = 0.1076e^{0.9802w}$ ($R^2 = 0.99$).

(4) Numerical simulation results are valid only for tested mudstone, for the specific compressive strength, Young modulus and Drucker-Prager parameters, and state of stress by depth of 800 m. The critical moisture level for other rocks may vary. However, the physics of the process obviously will not change. To obtain adequate results, the individual relationship between moisture content and mechanical parameters for a tested rock should be determined first. At the same time, heterogeneity of sedimentary rocks often does not allow to make the precise floor heave prediction along the roadway.[66]

4. Grouting reinforcement of floor heave

Over the last time, grouting reinforcement has been widely applied in mining for stability of roadways. Grouting provides improving of the mechanical parameters of the soft surrounding rock and reduces their permeability. The reinforcement of the floor rocks leads to a decrease in heaving.[18,19]

4.1. Mechanical parameters of grouting reinforced mudstone

Xu and Jiang[67] carried out the unconfined compression strength tests and triaxial compression tests on the common and reinforced mudstones. The results of tests show that during grouting of the mudstone speciments, the unconfined compressive strength increased by 108.4%, the elastic modulus increased by 273.1%, the shear modulus increased by 246.2%, and the cohesion increased by 62.3%, which indicate that the strengthened effect of the grouting is significant.

Zolfaghari et al.[68] used the geotechnical in-situ tests to evaluate the amount of improvement in mechanical properties of rock mass due to grouting reinforcement. Rock masses in the different boreholes at the grouting panels were tested and rock mass deformation modulus was calculated for each borehole. It was found, that after grouting the deformation modulus of Sv2 and Sv3 units in the left abutment (GL1 panel) increased by 242% and 209%, respectively and in the right abutment (GR2 panel) increased by 240%.

Utsuki[69] executed dilatometer tests of diferent rock types before and after grouting and examined the effect of improvement about the deformability of rock. It was shown, that after the grouting, the modulus of deformation is larger than before grouting at all the points. The ratio about the modulus of deformation before and after grouting was in the range of 1–10 for most of the experiments.

Zhang and Shimada[19] proposed the four grouting schemes where only the residual cohesion and friction angle were present. With the fourth (the most efficient) grouting scheme, the residual cohesion increases from 0 to 0.9 MPa and the friction angle increases from 22 to 26°.

The conducted analysis shows that the rate of improvement of rock mass properties during grounding determined on the initial properties of the rocks. In particular, for mudstone the deformation modulus increases by at least 2–2.4 times, the friction angle increases by 18%. Based on these studies, the mudstone parameters after grouting were calculated. The dilatancy angle was taken equal to the angle of internal friction, which corresponded to the unfavorable option. As shown above, the critical moisture level is 3–3.5%. Therefore, we calculate the

Table 5
Mudstone parameters after grouting.

N°	Moisture content (%)	Deformation modulus (GPa)	Poisson's ratio	Cohesion value, (MPa)	Angle of internal friction (deg)	Dilatancy angle (deg)
1	3.5	1.80	0.3	4,3	28	28
2	4	1.416	0.3	3.23	27	27
3	4.5	1.2	0.3	2.87	26	26
4	5	1.008	0.3	2.63	25	25

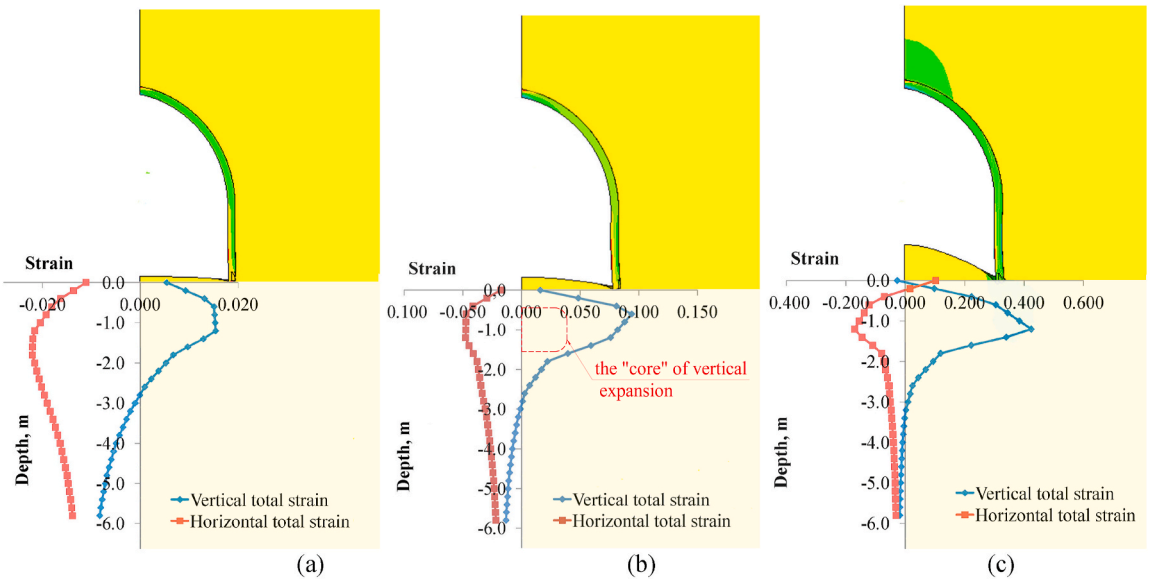

Fig. 14. The variation in horizontal and vertical total strains with depth under different moisture contents. (a) 3%; (b) 4%; (c) 5%.

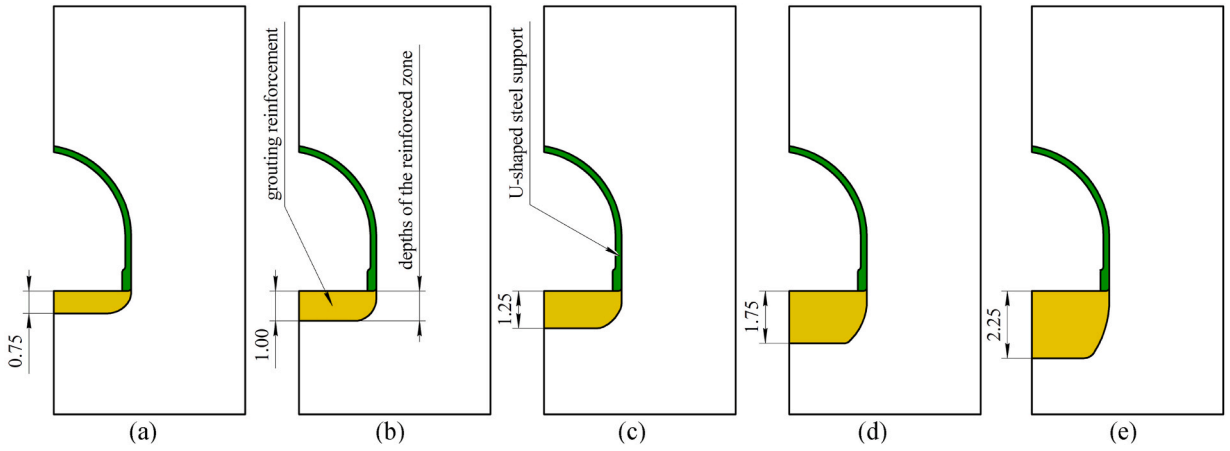

Fig. 15. The grouting schemes with different depth of reinforcement. (a) 0.75 m; (b) 1.0 m; (c) 1.25 m; (d) 1.75 m; (e) 2.25 m.

grouting reinforcement for moisture content of 3.5, 4, 4.5, 5% (Table 5).

4.2. Design of the grouting reinforcement scheme

In order to control the floor heave by a grouting method, the reinforced zone was constructed on the floor. Fig. 14 shows the variation of

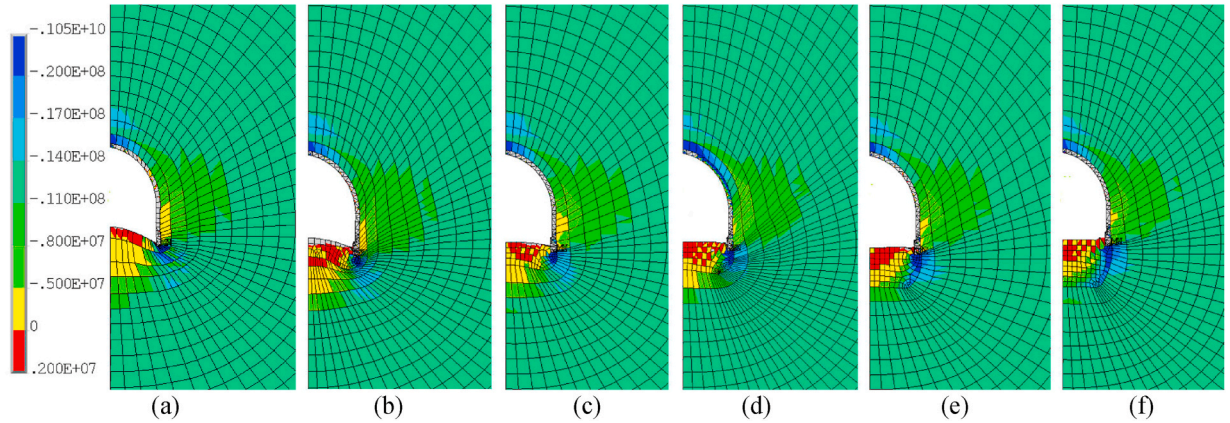

Fig. 16. Maximum principle stress distribution around the roadway before and after grouting with different depth of reinforcement (d_{rf}) (w = 5%). (a) before grouting; (b) d_{rf} = 0.75 m; (c) d_{rf} = 1.0 m; (d) d_{rf} = 1.25 m; (e) d_{rf} = 1.75 m; (f) d_{rf} = 2.25 m.

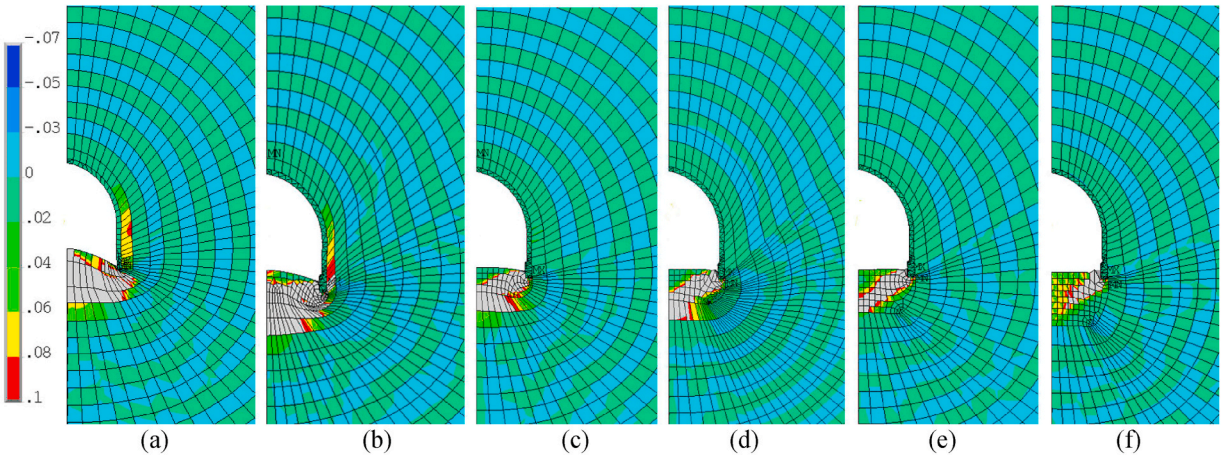

Fig. 17. Maximum principle strain distribution around the roadway before and after grouting with different depth of reinforcement (d_{rf}) (w = 5%). (a) before grouting; (b) d_{rf} = 0.75 m; (c) d_{rf} = 1.0 m; (d) d_{rf} = 1.25 m; (e) d_{rf} = 1.75 m; (f) d_{rf} = 2.25 m.

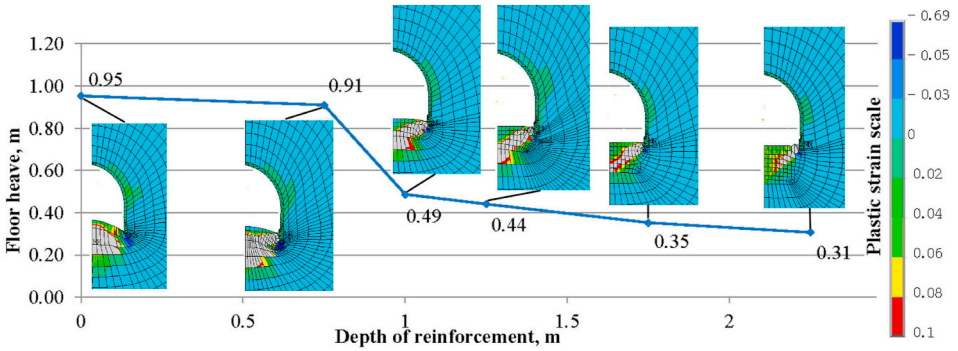

Fig. 18. Maximum floor heave and vertical plastic strain distribution around the roadway with different depth of reinforcement (w = 5%).

the strain in the floor of a roadway at the different moisture contents. As can be seen at 3% moisture content, the vertical strains are less than the critical ones (+0.02), while the horizontal compressive strains reach than the critical ones (−0.02).

In the case when the moisture content is more than 3%, the variation of the strain near the roadway floor has a non-linear nature. In this case, a "core" of vertical expansion appears. At 4% moisture content, both strains exceed post-peak ones. It can be seen that the depth of non-linear increase of strains is limited to 0.5–1.75 m. Thus, grouting reinforcement is advisable at the specified depth.

Fig. 15 shows the support pattern of the cross-cut with reinforcement. To investigate the effect of the grouting depth, five depths of the reinforced zone were simulated, such as 0.75 m, 1.0 m, 1.25 m, 1.75 m and 2.25 m. The optimal grouting scheme provides acceptable floor heave with a minimum depth and, accordingly, a minimum consumption of grouting material.

4.3. Effectiveness of grouting reinforcement

Figs. 16 and 17 show the distributions of maximum principle stress

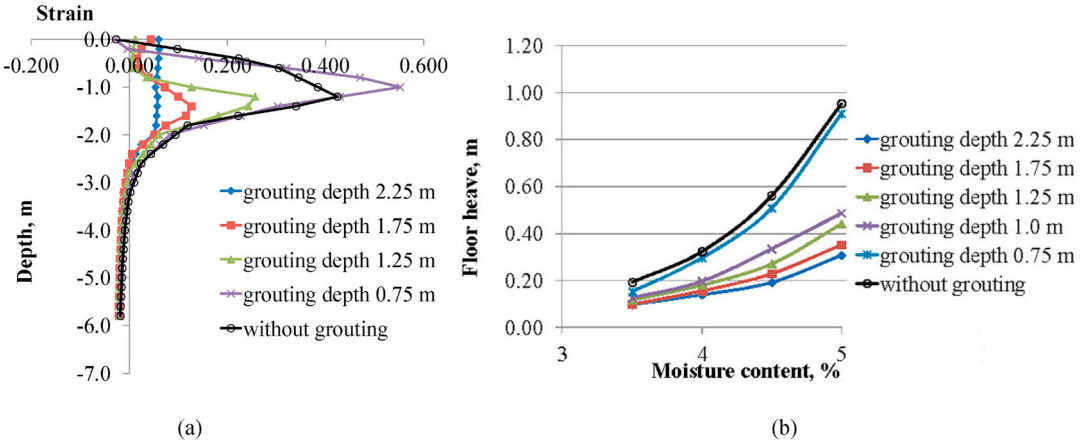

Fig. 19. The variation in vertical total strains with distance from the floor contour at different grouting depths (w = 5%) (a); influence of moisture content on the floor heave with different grouting depth (b).

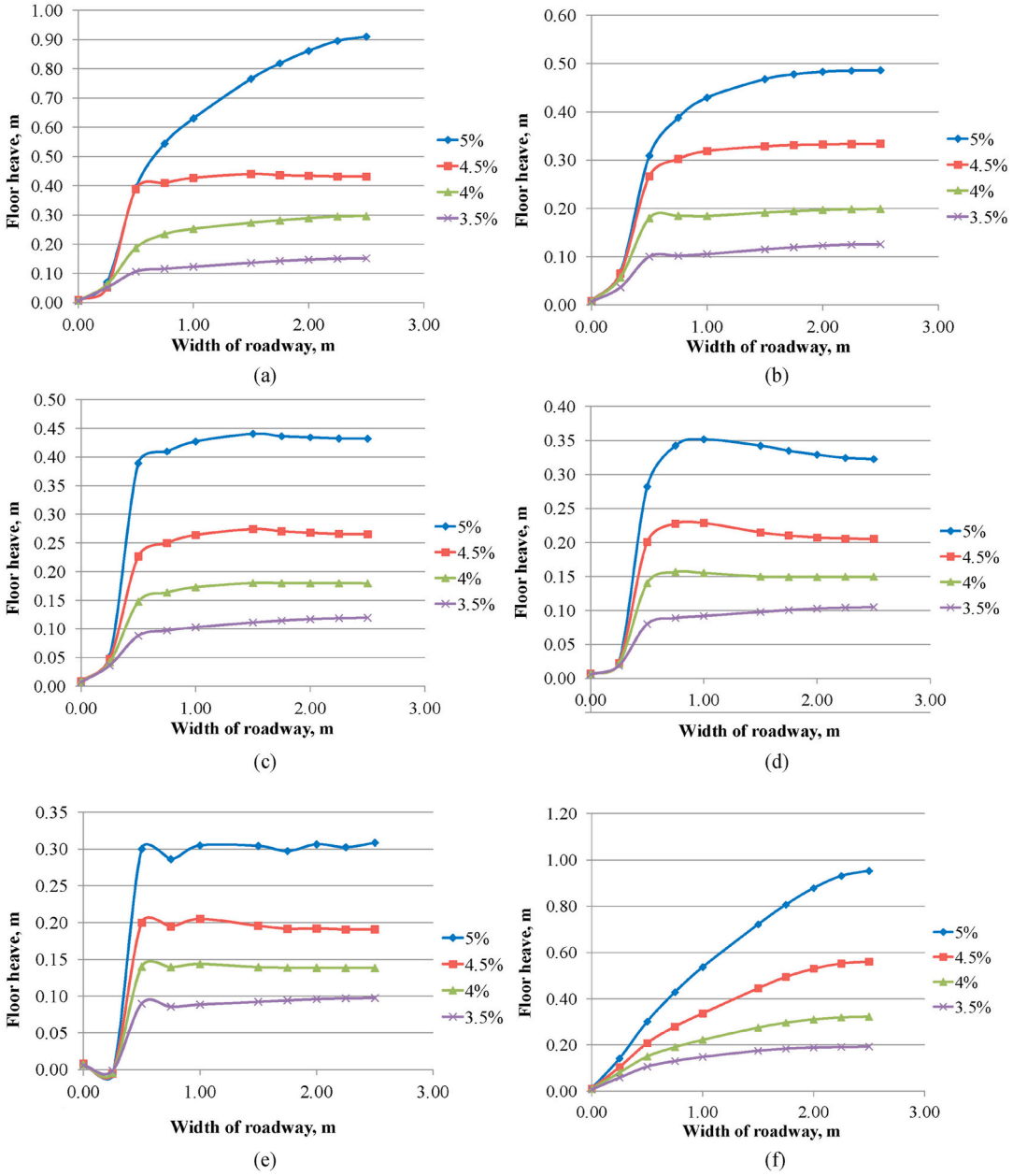

Fig. 20. Floor heave under different moisture contents before and after grouting with different depth of reinforcement (d_{rf}). (a) $d_{rf} = 0.75$ m; (b) $d_{rf} = 1.0$ m; (c) $d_{rf} = 1.25$ m; (d) $d_{rf} = 1.75$ m; (e) $d_{rf} = 2.25$ m; (f) before grouting.

and maximum principle strain respectively, for the surrounding rock under moisture content (w) 5% before and after grouting with different depth of reinforcement (d_{rf}).

The analysis of maximum principal stresses (σ_1) distribution after grouting (Fig. 15) shows that the size and configuration of the reduced stress zones in the surrounding rocks changed. In the side walls of the roadway, the (σ_1) does not change significantly. Along the side contour of the grouting zone, high compressive stresses are distributed, which, before grouting, appeared only in the corner under the leg of the support frame. In the roof of the roadway, the (σ_1) do not change significantly. In the floor of the roadway, the zone of reduced stresses decreased compared with the case without reinforcing. Below the reinforced area in the surrounding rocks for schemes with depth of reinforcement less than 1.75 m, a zone of reduced stress is also formed.

These stresses cause the maximum principal strain, that significantly exceeds the post-peak strains below the reinforced zone, as can be seen in Fig. 16. The size of the fracture zone decreases with increasing depth of grouting. Grouting to a depth of less than 1.75 m does not prevent the formation of a "core" of vertical expansion in the roadway floor, although it reduces its size, which has a positive effect on the stability of the floor.

Fig. 18 shows the evolution of max floor heave and vertical plastic strain distribution with different depth of reinforcement of surrounding rock under moisture content 5%. It is seen that a significant reduction in heaving is observed at a depth of reinforcement of more than 1.0 m. Although at a depth of reinforcement of less than 1.75 m below the reinforced zone, positive plastic strain still forms. The evolution of the vertical total strain with increasing of grouting depth is shown in Fig. 19 a. As can be seen, an increase in the grouting depth leads not only to a change in the location of the maximum strains, namely, to a displacement of them to the depth, but also to a decrease in absolute value of strains. In this case, the vertical strains at a grouting depth of 0.75 m are even greater in the local area under the reinforced zone, than in the case without grouting (see Fig. 20).

(a) (b)

Fig. 21. Floor heave. (a) in ventilation cross-cut after using a concrete beam; (b) in main ventilaton cross-cut after grouting with depth of reinforcement 1.75 m.

The effectiveness of reinforcing on the floor heave can be traced from the graphs shown in Fig. 19 b. The minimum required grouting depth is determined by the allowable level of floor heave and moisture content.

As can be seen from Fig. 19 b, grouting significantly reduces floor heave at any moisture content. An exception is the case when the depth of the reinforced zone is 0.75 m. In this case, the effect of grouting is invisible.

Floor heave evolutions along the width of roadway under different moisture contents before and after grouting are shown in Figure 20. It can be seen that as a result of grouting, the nature of heaving changes along the width of the roadway. The reinforced zone is displaced approximately uniformly in width, only the legs of the support frame are pressed into the roadway floor. In the reinforced zone, dilatancy and plastic flows are much less pronounced. The shape of floor contour after floor rock reinforcement was changed.

The insufficient depth of reinforcement does not have the significant effect on floor heave reduction, which is confirmed by the results of the study. This explains the negative effect of using a 0.5 m deep concrete beam in the ventilaton cross-cut to control floor heave. This technology was used in Surgaya coal mine, but it was not efficient. A concrete beam in the floor was squeezed out into a roadway and failured (Fig. 21 a).

Based on the stress and strain distributions, failure characteristics of the surrounding rock, a grouting method with a depth of reinforcement 1.75 m was proposed to stability the floor in c. The length of the experimental area in the roadway was 20 m. Grouting holes with diameter 42 mm were drilled vertical on a square grid with a step of 1.2 m. The portland slag cement type PC-IIB/SH-400 (Blaine 2.9–3.1 m^2/g) with W:C ratio of 0.5:1 and 0.75 l super-plasticizer SikaBV per 100 kg was injected in floor boreholes with pneumatic grouting pump machine. Grouting pressure varied from 5 to 8 bars on different depth. To evaluate the reinforcing effect, two measuring stations were arranged in the crosscut. Three measuring piles were arranged on the roof, floor, and middle of the roadway sides of each measuring station. The “cross measurement method“ was used to measurement of the floor heave. The time of monitoring was 200 day.

For station 1, the maximum of vertical convergence and the floor heave were 409 mm and 330 mm respectively. For station 2, the maximum of vertical convergence and the floor heave were 415 mm and 322 mm respectively. The floor heave was three times less than without grouting. Deformations of the roof and floor of roadway suggest that grouting renforcement has a good effect. A photo of the crosscut at the experimental area is shown in Figure 21 **b**. Although the grouting method is quite expensive, with large water inflows from the floor of the roadway (for example as can be seen in Fig. 1) it is reasonable. Under such conditions, both bolting and usage of concrete beams do not prevent extreme floor heave.

5. Conclusions

In this study, roadway in soft rock containing the mine water was considered as the research subject. We focused on the floor heave evolution and the effectiveness of grouting reinforcement of single roadway. A numerical simulation was used to study the stress and strain distributions of the surrounding rock on the underground coal mine 800 m in depth of Ukraine. The results demonstrated that significant floor heave was caused plastic deformation of mudstone under high moisture content. This was followed by investigating the mechanism of non-linear floor heave and grouting reinforcement. Based on the results of this investigation, the following conclusions can be drawn.

(1) The compressive strength and friction angle linearly decrease with the increase of moisture content. The deformation modulus and cohesion decrease exponentially with the increase of moisture content. Therefore, the influence of mine water should be considered at the design stage of the support system of roadway.
(2) The numerical analysis shows that the size of the zone of reduced stress in the floor and the sidewalls of the roadway increases gradually. At the same time, as the zone of reduced stress in the floor increase, in the wall sides of the roadway, the stresses become less intense. The critical moisture level for mudstone is 3–3.5%. An active increase in maximum principle stress and plastic strain, which are the cause of uncontrolled dramatic floor heave, starts at this limit. In the floor of roadway, vertical failure strains are positive, at the same time horizontal ones are negative. In the case of large floor heave a “core” of vertical expansion is formed in the floor strata. This area of the surrounding rocks is mainly involved in the development of floor heave. For each rock, the limit moisture content, which is influenced by the type of rock, its mechanical properties and stress-strain state, can be found. Exceeding of this limit causes the acceleration of deformations around the roadway.
(3) Considering the floor heave mechanism of the soft rock containing the mine water, grouting reinforcement was proposed to control the floor heave. Five grouting schemes with different depth of reinforcement were studied during many numerical simulations. After grouting reinforcement, plastic strain in the floor strata was reduced effectively. The minimum required grouting depth is determined by the allowable floor heave and moisture content. Ideally, the floor heaves could be reduced when the grouting depth is greater than the area where the “core” of vertical expansion appears. This can provide suggestions for the depth of reinforcement selection during floor heave control through grouting reinforcement technology.

(4) Correctly selected roadway support system is one of the most important issues in mining technology that plays a key role in ensuring of the operation effectiveness and safety of production. The floor heave is a serious failure phenomenon in mine roadways, especially in conditions of increased water inflows. The floor heave control by grouting reinforcement is width commonly practice. Conducted studies in the conditions of Ukrainian mine expand the understanding of the effectiveness of floor grouting in conditions of high water inflows. The obtained results make it possible to improve the grouting reinforcement of floor technology.

Declaration of competing interest

The authors declare that they have no known competing financial interests or personal relationships that could have appeared to influence the work reported in this paper.

Data availability

No data was used for the research described in the article.

References

1 Ritchie Hannah, Roser Max. Energy. *Published online at OurWorldInData.org*; 2020. https://doi.org/10.1016/j.ijmst.2012.04.0021. https://ourworldindata.org/energy.
2 Sungsoon M, Kudret T, Serkan S. Management of floor heave at Bulga Underground Operations—a case study. *Int J Min Sci Technol*. 2019;29:73–78. https://doi.org/10.1016/j.ijmst.2018.11.015.
3 Shi J, Kong D. Floor heave mechanism and anti-slide piles control technology in deep and large-span chamber. *Appl Sci*. 2021;11(10):4576.
4 Jia H, Wang L, Fan K, Peng B, Pan K. Control technology of soft rock floor in mining roadway with coal pillar protection: a case study. *Energies*. 2019;12(15):3009.
5 Skrzypkowski K, Zagórski K, Zagórska A, et al. Choice of the arch yielding support for the preparatory roadway located near the fault. *Energies*. 2022;15(10):3774. https://doi.org/10.3390/en15103774.
6 Chen YG, Lu SL. *Surrounding Rock Control of Coal Mine Roadway in China*. Xuzhou, China: China University of Mining & Technology Press; 1994:463–473.
7 Zhang D, Bai J, Yan Sh, Wang R, Meng N, Wang G. Investigation on the failure mechanism of weak floors in deep and high-stress roadway and the corresponding control technology. *Minerals*. 2021;11(12):1408. https://doi.org/10.3390/min11121408.
8 Perry KA, Bradley J, Unrug KF, Klimek M. Mitigation of floor heave in west Kentucky coal mine. *Int J Min Sci Technol*. 2016;26:521–525.
9 Zhao YM, Liu N, Zheng X, Zhang N. Mechanical model for con-trolling floor heave in deep roadways with U-shaped steel closed support. *Int J Min Sci Technol*. 2015;25:713–720. https://doi.org/10.1016/j.ijmst.2015.07.003.
10 Wang C, Wang Y, Lu S. Deformational behaviour of roadways in soft rocks in underground coal mines and principles for stability control. *Int J Rock Mech Min Sci*. 2000;37:937–946. https://doi.org/10.1016/S1365-1609(00)00026-5.
11 Wu L, An L, Bai Y. In-plane stability of steel circular closed supports with I-section of sinusoidal corrugated webs: experimental and numerical study. *Tunn Undergr Space Technol*. 2020;106(8), 103566. https://doi.org/10.1016/j.tust.2020.103566.
12 Chen A, Li XB, Liu XS, Tan YL, Xu K, Wang HL. Relief-retaining control technology of floor heave in mining roadway with soft rock: a case study. *Adv Civ Eng*. 2021;2021. https://doi.org/10.1155/2021/1455052. Article ID 1455052, 13.
13 Guo ZP, Du ZW, Hu SC. Comprehensive treatmentmethods of floor heave disasters in mining areas of China. *Geotech Geol Eng*. 2017;35(5):2485–2495. https://doi.org/10.1007/s10706-017-0250-8.
14 He MC, Zhang GF, Wang GL, Xu YL, Wu CZ, Tang QD. Research on mechanism and application to floor heave control of deep gateway. *Chin J Rock Mech Eng*. 2009;28:2593–2598.
15 Yang J, Zhou K, Cheng Y, Gao Y, Wei Q, Hu Y. Mechanism and control of roadway floor heave in the paleogene soft rock surroundings. *Geotech Geol Eng*. 2019;37(6):5167–5185. https://doi.org/10.1007/s10706-019-00970-6.
16 Wang Y, Wang P, Li W, et al. Floor heave control technology in deep and soft rock mining roadway: a case study. *Arabian J Geosci*. 2022;15:500. https://doi.org/10.1007/s12517-022-09765-1.
17 Chang Q, Zhou H, Xie Z, Shen S. Anchoring mechanism and application of hydraulic expansion bolts used in soft rock roadway floor heave control. *Int J Min Sci Technol*. 2013;23(3):323–328. https://doi:10.1016/j.ijmst.2013.05.017.
18 Shimada H, Hamanaka A, Sasaoka T, Matsui K. Behaviour of grouting material used for floor reinforcement in underground mines. *Int J Min Reclamat Environ*. 2014;28(2):133–148. https://doi.org/10.1080/17480930.2013.804257.
19 Zhang ZY, Shimada H. Numerical study on the effectiveness of grouting reinforcement on the large heaving floor of the deep retained goaf-side gateroad: a case study in China. *Energies*. 2018;11:1001. https://doi.org/10.3390/en11041001.
20 Gong P, Ma Z, Ni X, Zhang RR. Floor mechanism of gob-side entry retaining with fully-mechanized backfilling mining. *Energies*. 2017;10(12):2085.
21 Zhu C, Wang Y, Chen M, Chen Z, Wang Hm. Mechanics model and numerical analysis of fioor heave in soft rock roadway. *J Coal Sci Eng*. 2011;17(4):372–376.
22 Tang SB, Tang CA. Numerical studies on tunnel floor heave in swelling ground under humid conditions. *Int J Rock Mech Min Sci*. 2012;55:139–150.
23 Sun X, Chen F, He M. Physical modeling of floor heave for the deep-buried roadway excavated in ten degree inclined strata using infrared thermal imaging technology. *c*. 2017;63:228–243.
24 Zhong Z, Tu Y, Liu X. Occurrence mechanism and control technology of the floor heave disaster for soft-rock tunnel. *Disaster Adv*. 2012;5:987–992.
25 Zhu L, Yao QL, Xia Z, Wang WN, Li XH. Study on the movement characteristics of the overlying stratum and surrounding rock control in ultraclose coal seams: a case study. *Energy Sci Eng*. 2020;8(4):1231–1246.
26 Sakhno I, Sakhno S, Kamenets V. Mechanical model and numerical analysis of a method for local rock reinforcing to control the floor heave of mining-affected roadway in a coal mine. *IOP Conf Ser Earth Environ Sci*. 2022;970(1), 012035. https://doi.org/10.1088/1755-1315/970/1/012035.
27 ISRM (International Society for Rock Mechanics). In: Brown ET, ed. *Suggested Methods for Rock Characterization Testing and Monitoring*. Oxford Pergamon Press; 1981:211.
28 Kanji MA. Critical issues in soft rocks. *J. Rock Mech. Geotech*. 2014;6:186–195.
29 Li D, Wang W. Quantitative analysis of the influence of saturation on rock strength reduction considering the distribution of water. *Geomech. Geophys. Geo- Energy Geo-Resources*. 2019;5(2):197–207. https://doi.org/10.1007/s40948- 019-00106-3.
30 Zhu Z, et al. Overburden movement characteristics of top-coal caving mining in multi-seam areas. *Q J Eng Geol Hydrogeol*. 2018;51(2):276. https://doi.org/10.1144/qjegh2017-076.
31 Sakhno I, Isayenkov O, Rodzin S. Local reinforcing of footing supported in the destroyed rock massif. *Mining of Mineral Deposits*. 2017;11(1):9–16. https://doi.org/10.15407/mining11.01.009.
32 Shakoor A, Barefield EH. Relationship between unconfined compressive strength and degree of saturation for selected sandstones. *Environ Eng Geosci*. 2009;15(1):29–40. https://doi.org/10.2113/gseegeosci.15.1.29.
33 Verstrynge E, Adriaens R, Elsen J, Van Balen K. Multi-scale analysis on the influence of moisture on the mechanical behavior of ferruginous sandstone. *Construct Build Mater*. 2014;54:78–90. https://doi.org/10.1016/j. conbuildmat.2013.12.024.
34 Heap MJ, Villeneuve M, Kushnir ARL, Farquharson JI, Baud, Reuschl'e PT. Rock mass strength and elastic modulus of the Buntsandstein: an important lithostratigraphic unit for geothermal exploitation in the Upper Rhine Graben. *Geothermics*. 2019;77:236–256. https://doi.org/10.1016/j.geothermics.2018.10.003.
35 Lashkaripour GR, Ajalloeian R. The effect of water content on the mechanical behaviour of fine-grained sedimentary rocks. *ISRM Int. Symp.*. 2000.
36 Jiang Q, Cui J, Feng X, Jiang Y. Application of computerized tomographic scanning to the study of water-induced weakening of mudstone. *Bull Eng Geol Environ*. 2014;73(4):1293–1301. https://doi.org/10.1007/s10064-014-0597- 5.
37 Erguler ZA, Ulusay R. Water-induced variations in mechanical properties of clay-bearing rocks. *Int J Rock Mech Min Sci*. 2009;46(2):355–370.
38 Rabat 'A, Tom'as R, Cano M, Miranda T. Impact of water on peak and residual shear strength parameters and triaxial deformability of high-porosity building calcarenite stones: interconnection with their physical and petrological characteristics. *Construct Build Mater*. 2020;262:1–20. https://doi.org/10.1016/j.conbuildmat.2020.120789.
39 Chen Y, Li Q, Pu H, et al. Modeling and simulation of deformation mechanism of soft rock roadway considering the mine water. *Geofluids*. 2020;2020, 8812470.
40 Sakhno IG, Molodetskyi AV, Sakhno SV. Identification of material parameters for numerical simulation of the behavior of rocks under true triaxial conditions. *Naukovyi Visnyk NHU*. 2018;5:48–53. https://doi.org/10.29202/nvngu/2018-5/4.
41 Cherblanc F, Berthonneau J, Bromblet P, Huon V. Influence of water content on the mechanical behaviour of limestone: role of the clay minerals content. *Rock Mech. Rock*. 2016;49(6):2033–2042. https://doi.org/10.1007/s00603-015- 0911-y.
42 Masoumi H, Horne J, Timms W. Establishing empirical relationships for the effects of water content on the mechanical behavior of gosford sandstone. *Rock Mech Rock Eng*. 2017;50(8):2235–2242. https://doi.org/10.1007/s00603- 017-1243-x.
43 Vergara MR, Triantafyllidis T. Influence of water content on the mechanical properties of an argillaceous swelling rock. *Rock Mech Rock Eng*. 2016;49(7):2555–2568. https://doi.org/10.1007/s00603-016-0938-8.
44 Rabat 'A, Tom'as R, Cano M. Evaluation of mechanical weakening of calcarenite building stones due to environmental relative humidity using the vapour equilibrium technique. *Eng Geol*. 2020;278:1–20.
45 Zhou Z, Cai X, Cao W, Li X, Xiong C. Influence of water content on mechanical properties of rock in both saturation and drying processes. *Rock Mech Rock Eng*. 2016;49(8):3009–3025. https://doi.org/10.1007/s00603-016-0987-z.
46 Romana M, V'as'arhelyi B. A discussion on the decrease of unconfined compressive strength between saturated and dry rock samples. *Proc. 11th Congr. Int. Soc. Rock Mech*. 2007;1:139–142.
47 AL-Bazali T. The impact of water content and ionic diffusion on the uniaxial compressive strength of shale. *Egypt. J. Pet*. 2013;22:249–260. https://doi.org/10.1016/j.ejpe.2013.06.004.
48 Malkowski P, Ostrowski L, Bozecki P. The impact of the mineral composition of Carboniferous claystones on the water-induced changes of their geomechanical properties. *Geology, Geophysisc and Environment*. 2017;43(1):43–55.
49 Małkowski P, Ostrowski Ł, Stasica J. Modeling of floor heave in underground roadways in dry and waterlogged conditions. *Energies*. 2022;15(12):4340.
50 Wang WJ, Yuan C, Guo GY, Yu WJ. Control of malignant expansion of plastic zone in surrounding rock of rock roadway under the conditions of violent mining. *J Min Saf Eng*. 2016;33(6):957–964.

51 Abdel-Meguid M, Rowe RK, Lo KY. Three-dimensional analysis of unlined tunnels in rock subjected to high horizontal stress. *Can Geotech J*. 2003;40(6):1208–1224.
52 Leitman MJ, Villaggio P, Leitman MJ, Villaggio P. Plastic zone around circular holes. *J Eng Mech*. 2009;135(12):1467–1471.
53 Huang Y, Zhao A, Zhang T, Guo W. Plastic failure zone characteristics and stability control technology of rodway in the fault area under non-uniformly high geostress: a case study from Yuandian coal mine in Northern Anhui Province, China. *Open Geosci*. 2020;12(1):406–424. https://doi.org/10.1515/geo-2020-0154.
54 Yuan Y, Wang W, Li S, et al. Failure mechanism for surrounding rock of deep circular roadway in coal mine based on mining-induced plastic zone. *Adv Civ Eng*. 2018;2018:1–14.
55 Zhang JH, Wang LG, Li QH, Zhu SS. Plastic zone analysis and support optimization of shallow roadway with weakly cemented soft strata. *Int J Min Sci Technol*. 2015;25(3):395–400.
56 Li C, Xu JH, Pan JZ, Ma C. Plastic zone distribution laws and its types of surrounding rock in large-span roadway. *Int J Min Sci Technol*. 2012;22(1):23–28.
57 Gao GY, Chen QS, Zhang QS, Chen GQ. Analytical elasto-plastic solution for stress and plastic zone of surrounding rock in cold region tunnels. *Cold Reg Sci Technol*. 2012;72:50–57.
58 Sugimoto S, Ochiai H, Yasufuku N, Kawamura A, Imanishi H. *Estimation of extended plastic zone in the ground with the deformation of cylindrical cavity*. 2004;19:383–384.
59 Xiang YY, Feng SQ. Teoretical prediction of the potential plastic zone of shallow tunneling in vicinity of pile foundation in soils. *Tunn Undergr Space Technol*. 2013;38:115–121.
60 Liu Q, Fu Q, Yang K, Wei Q, Liu H, Wu H. Geomechanical modeling and inversion analysis of the in-situ stress field in deep marine shale formations: a case study of the lo*ngmaxi* formation, dingshan area, China. *Front Earth Sci*. 2022;9. Article 808535.
61 Sakhno I., Sakhno S. Numerical Studies of Floor Heave Control in Deep Mining Roadways with Soft Rocks by the Rock Bolts Reinforcement Technology, Adv. Civ. Eng. 2023; 2023, Article ID 2756105. https://doi.org/10.1155/2023/2756105.
62 Zhou H, Zhang C, Li Z, Hu D, Hou J. Analysis of mechanical behavior of soft rocks and stability control in deep tunnels. *J Rock Mech Geotech Eng*. 2014;6(3):219–226.
63 Josh M, Esteban L, Delle Piane C, Sarout J, Dewhurst DN, Clennell MB. Laboratory characterisation of shale properties. *J Petrol Sci Eng*. 2019;88–89:107–124.
64 Almisned OA, Alqahtani N. Rock analysis to characterize Saudi soft sandstone rock. *J Pet Explor Prod Technol*. 2021;11(6):2381–2387.
65 Liu Q, Liang B, Sun W, Zhao H. Experimental study on the difference of shale mechanical properties. *Adv Civ Eng*. 2021;2021:1–14. Article ID 6677992.
66 Małkowski P, Ostrowski Ł, Bednarek Ł. The effect of selected factors on floor upheaval in roadways-in situ testing. *Energies*. 2020;13(21):5686.
67 Xu J, Jiang J. Experiment and application study on high-performance grouting material used to solve the floor heave problem of broken soft rocks. *Frontiers in Physics*. 2022. https://doi.org/10.3389/fphy.2022.829681, 10 Article 8296811.
68 Zolfaghari A, Bidar AS, Javan MM, Haftani M, Mehinrad A. Evaluation of rock mass improvement due to cement grouting by Q-system at Bakhtiary dam site. *Int J Rock Mech Min Sci*. 2015;74:38–44.
69 Utsuki S. In-situ experimental studies on improvement of deformability of rock masses by grout treatment. *Jpn Comm Rock Mech*. 2013;9:7–8.